Journal of Global Biogeochemical Cycles

Supporting Information for

Quantifying the role of seasonality in the marine carbon cycle feedback: an ESM2M case study

Andrea J. Fassbender[1,2], Sarah Schlunegger[3], Keith B. Rodgers[4,5], John P. Dunne[6]

[1]Monterey Bay Aquarium Research Institute, Moss Landing, California, USA
[2]Now at: NOAA/OAR Pacific Marine Environmental Laboratory, Seattle, WA, USA
[3]Program in Atmospheric and Oceanic Sciences, Princeton University, Princeton, New Jersey, USA
[4]Center for Climate Physics, Institute for Basic Science, Busan, South Korea
[5]Pusan National University, Busan, South Korea
[6]NOAA/OAR Geophysical Fluid Dynamics Laboratory, Princeton, NJ, USA

Contents of this file

Introduction

This file includes information about how carbonate system internal consistency is ensured when using model output variables in offline MATLAB calculations. This file also includes information about the bias-correction of reconstructed pCO_2 values prior to sea-air flux calculation, as well as our method to enhance the accuracy of offline sea-air flux calculations through use of an effective gas transfer velocity. The file also includes twelve supporting figures, each of which is referenced in the main text. Additional details regarding the model data and offline calculations can be found in the *Description of Model Data and Carbonate System Calculations* and *Methodology* sections of the main text.

Text S1.

Monthly output of dissolved inorganic carbon (DIC), total alkalinity (TA), and carbon dioxide partial pressure (pCO_2) from GFDL ESM2M are required for this analysis. When DIC and TA are used to compute pCO_2 with the MATLAB program CO2SYS version 1.1 (van Heuven et al., 2011; Lewis & Wallace, 1998), notable differences between the model output and calculated pCO_2 values are found (**Fig. S1a**). These discrepancies, which are largest in the tropics and grow over time (**Fig. S1c**), are caused by different equilibrium constants for carbon dioxide solubility (K_0) being used in the CO2SYS and ESM2M ocmip2_co2calc code. CO2SYS uses the relationship of Weiss (1974) while ocmip2_co2calc uses the relationship of Weiss & Price (1980). Since our analysis requires offline calculations of pCO_2 and internal consistency of the carbonate system, we rectify this issue at the start of our analysis by recomputing DIC from monthly model output

of pCO_2, TA, salinity, temperature, phosphate, and silicate. The resulting DIC values are similar to the model output, with regional adjustments of up to ~10 µmol kg^{-1} DIC (**Fig. S1b**). By forcing internal carbonate system consistency at the monthly timescale, we ensure that calculated pCO_2 values in later methodological steps yield consistent air-sea pCO_2 disequilibrium with the model output.

Text S2.

Reconstructed transient pCO_2 values are in excellent agreement ($r = 0.99$, $p < 0.01$) with the model output pCO_2 values, with the largest biases found in the high latitudes (**Fig. S4** and **S5**). While globally the pCO_2 biases (-2.1±3.2 µatm, area-weighted mean over all time) are small relative to the background pCO_2 values and seasonal cycle amplitudes, they can have a nontrivial impact on sea-air CO_2 flux calculations and cumulative fluxes. To address this issue, we smooth the transient pCO_2 bias in each grid from 1950 to 2100 using a running mean filter with a 120-element (10-year) sliding window to isolate persistent decadal offsets between model output and reconstructed values. The smoothed bias is then added to each of the reconstructed pCO_2 time series, recentering them on $pCO_{2\,AM}$ plus the bias. This bias correction reduces the area-weighted mean difference (over all time) between model output and reconstructed transient pCO_2 to negligible values (< .01 µatm; ±2.5 uatm).

The bias-corrected, reconstructed pCO_2 values are then used to calculate sea-air CO_2 fluxes and quantify the magnitude and spatial structure of the overall seasonal carbon cycle feedback, as well as the individual driver contributions. The quadratic relationship between wind speed and gas exchange applied in ESM2M means that sea-air CO_2 fluxes computed with monthly mean, versus instantaneous, wind speeds will also have a bias (Monteiro et al., 2015; Wanninkhof, 2014). For example, relative to ESM2M output of monthly sea-air CO_2 fluxes, offline recomputed fluxes yield ~7% greater cumulative ocean carbon uptake by the end of the century (**Fig. S7**). To address this issue, we quantify effective monthly gas transfer velocities by dividing model output fluxes by model output ΔpCO_2 values. For each model grid, effective gas transfer velocities that exceed 10 times the 1950 to 2100 median value are set to that median value. Once large outliers are removed, remaining values exceeding ±3σ from the 1950 to 2100 mean value are set to that mean value. This process impacts <1.5% of the effective gas transfer velocities globally over all time, and the method yields excellent agreement ($r = 0.99$, $p < 0.01$) between the model output and our reconstructed transient sea-air CO_2 fluxes (**Fig. S6** and **S7**) with a 1% difference in cumulative ocean carbon uptake by the end of the century. This approach is used for all offline flux calculations in the analysis.

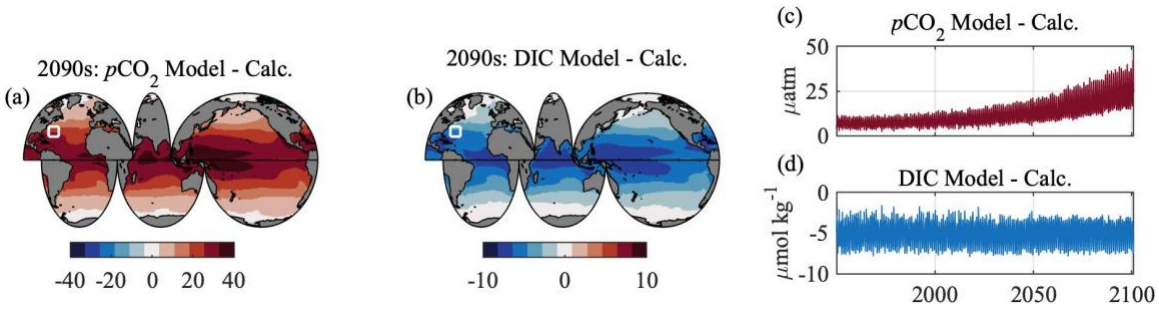

Figure S1. Difference between model output and values calculated from model output using the MATLAB program CO2Sys version 1.1 for (**a**) pCO_2 (µatm) and (**b**) DIC (µmol kg^{-1}). Time series of the (**c**) pCO_2 and (**d**) DIC differences at the model grid corresponding to the Bermuda Atlantic Time-series Study location (31.67°N 64.17°W), outlined with a white box on each map. Results from ensemble member 1 are shown.

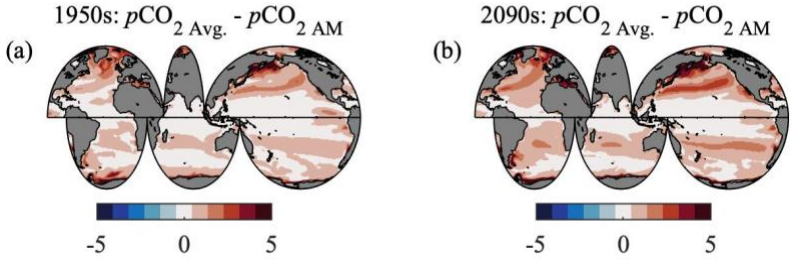

Figure S2. Difference between annual mean $pCO_{2\ Avg.}$ values ($pCO_{2\ Avg.}$) and $pCO_{2\ AM}$ values (µatm) for the (**a**) 1950s and (**b**) 2090s. Results from ensemble member 1 are shown.

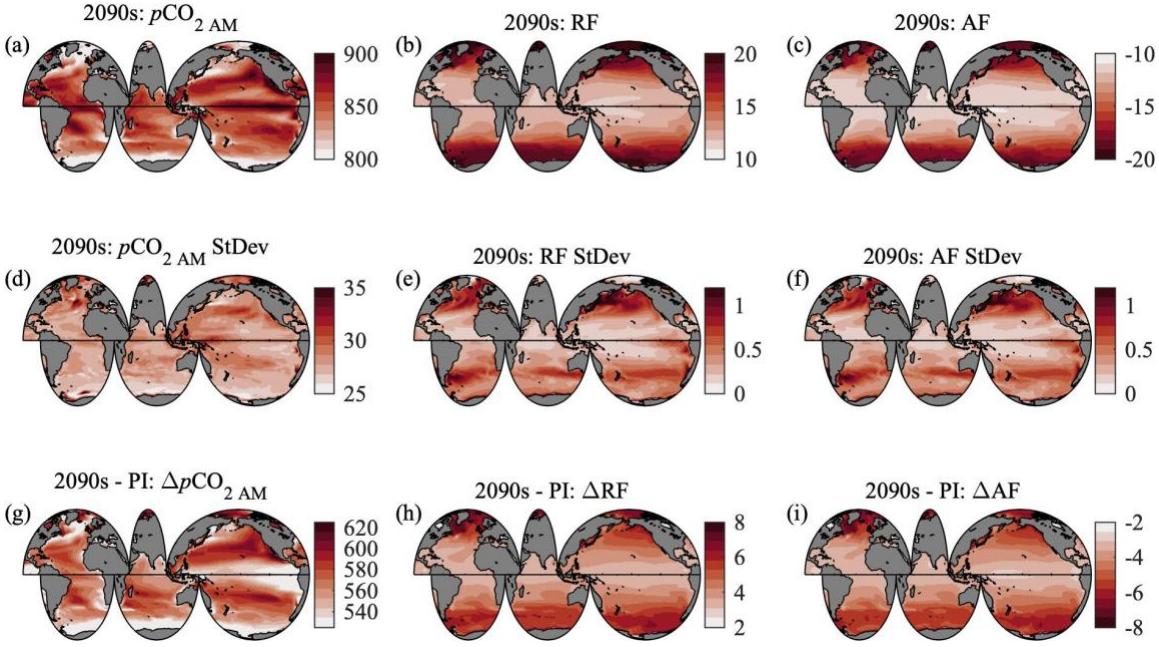

Figure S3. 2090s ensemble mean and standard deviation for (**a, d**) $pCO_{2\ AM}$ (µatm) (**b, e**) Revelle Factor (RF) and (**c, f**) Alkalinity Factor (AF) values. Change in (**g**) $pCO_{2\ AM}$ (µatm), (**h**) RF, and (**i**) AF values from the preindustrial period to the 2090s.

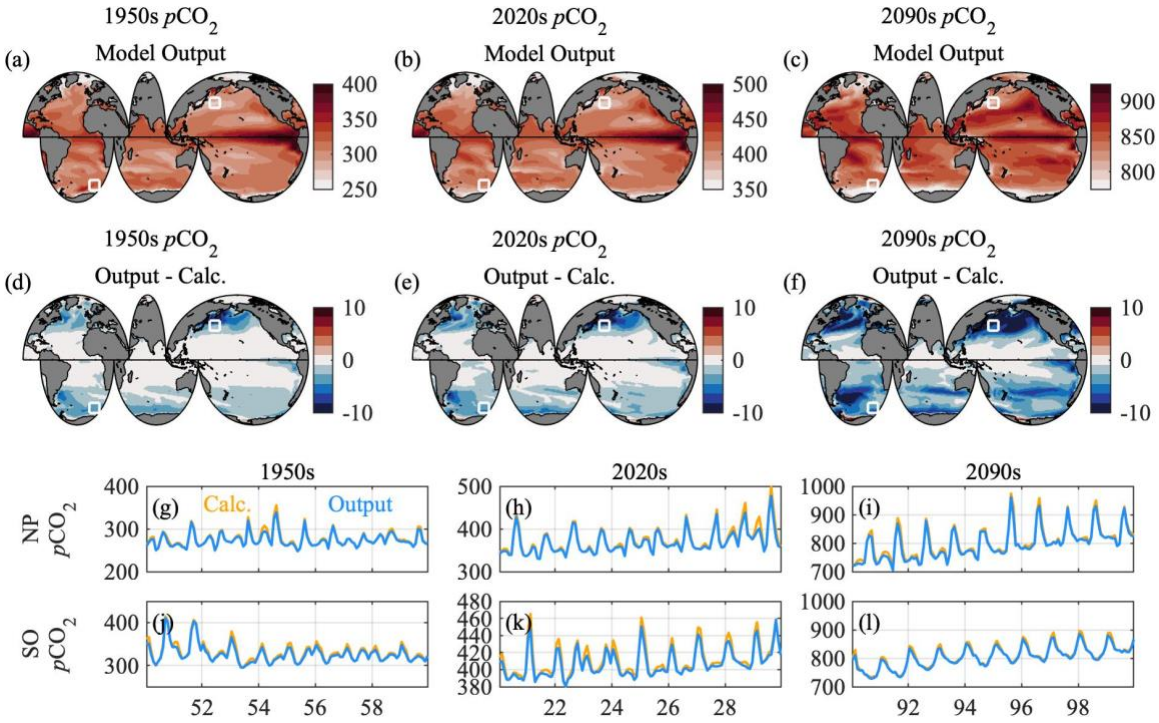

Figure S4. Decadal mean pCO_2 values (µatm) for the (**a**) 1950s, (**b**) 2020s, and (**c**) 2090s from model output. Difference between model output and reconstructed (Calc. = $pCO_{2\,T} + pCO_{2\,BP}$; prior to bias correction) values for the (**d**) 1950s, (**e**) 2020s, and (**f**) 2090s. Time series of model output and calculated values for the 1950s, 2020s, and 2090s at grid cells in the (**g-i**) North Pacific Ocean (159.5° E, 39.5° N) and (**j-l**) Southern Ocean (9.5° E, -58.5° N). Results from ensemble member 1 are shown.

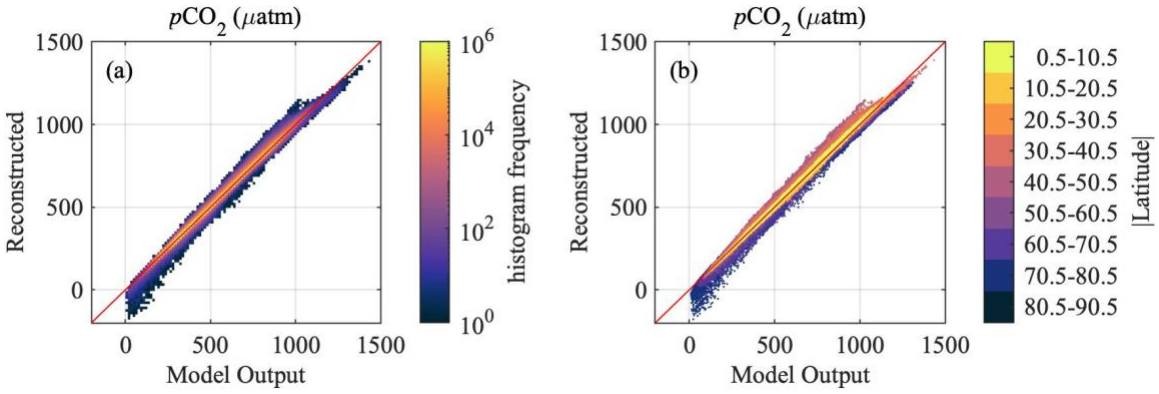

Figure S5. Relationship between model output and reconstructed (prior to bias correction) pCO_2 values. (**a**) Two-dimensional histogram showing the number of values that fall within bins of model output (x-axis) and reconstructed (y-axis) values. Lighter colors indicate more values per bin. The colorbar is logarithmic. (**b**) Values colored by absolute latitude. The red line in each subplot is the 1:1 line. Results from ensemble member 1 are shown.

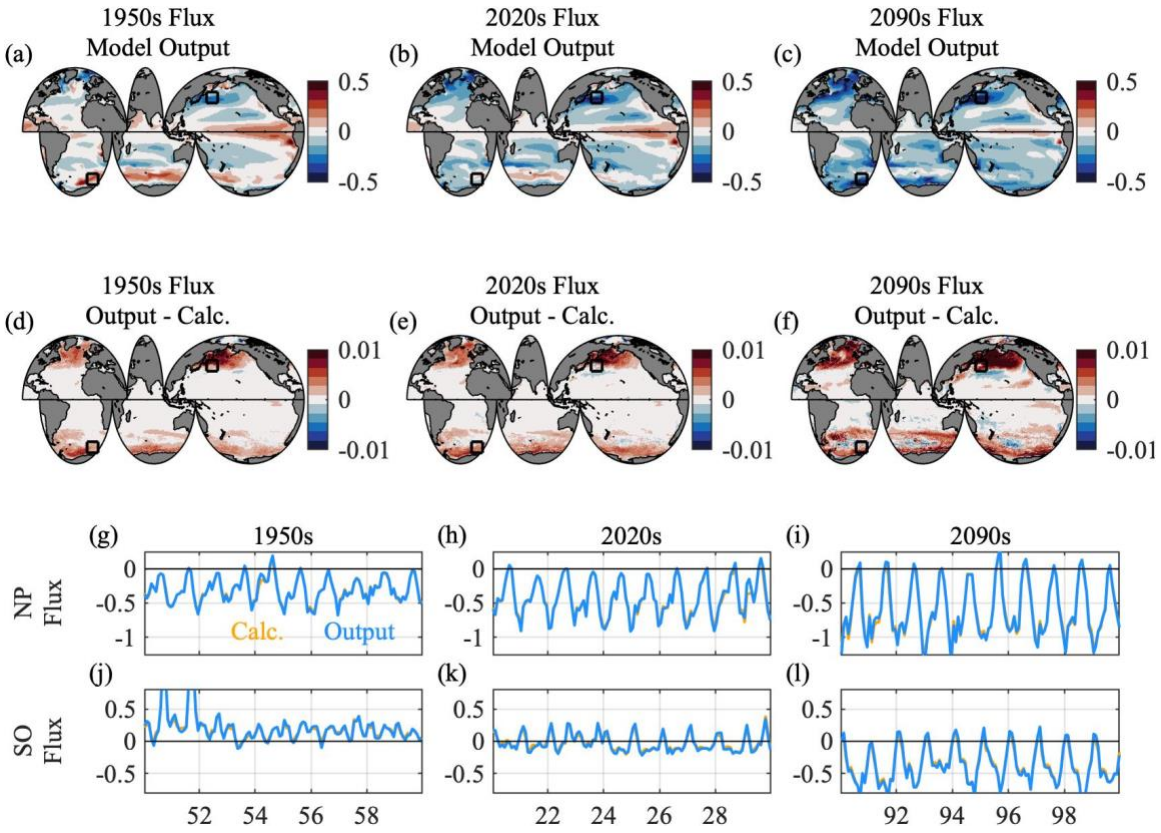

Figure S6: Decadal mean sea-air CO_2 fluxes (mol C m^{-2} $month^{-1}$) for the (**a**) 1950s, (**b**) 2020s, and (**c**) 2090s from model output. Difference between model output and calculated (Calc.) fluxes (using bias-corrected pCO_2 values and effective gas transfer velocities) for the (**d**) 1950s, (**e**) 2020s, and (**f**) 2090s. In the difference figures, red coloring indicates that calculated fluxes overestimate the sink or underestimate the source strength and blue coloring indicates that calculated fluxes underestimate the sink or overestimate the source strength. Time series of model output and calculated fluxes for the 1950s, 2020s, and 2090s at grid cells in the (**g-i**) North Pacific Ocean (159.5° E, 39.5° N) and (**j-l**) Southern Ocean (9.5° E, -58.5° N). Results from ensemble member 1 are shown.

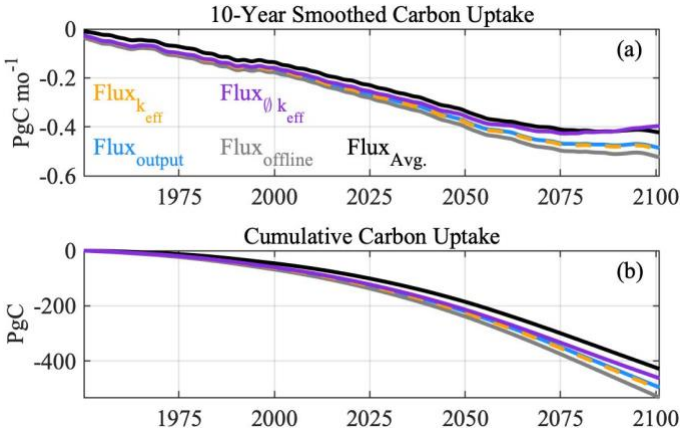

Figure S7. (**a**) Global carbon sink strength (PgC mo^{-1}) over time computed from: mode output ($Flux_{output}$); standard offline flux calculations using monthly model output of pCO_2 and wind speed ($Flux_{offline}$); and modified offline flux calculations using effective gas transfer velocities (k_{eff}) with our reconstructed, bias-corrected monthly transient ($Flux_{Keff}$) and no-leverage (Ø; $Flux_{\phi\ Keff}$) pCO_2 values as well as annually averaged ($Flux_{Avg.}$) model output pCO_2 values; and . (**b**) Cumulative sum of values shown in subplot **a**. Results from ensemble member 1.

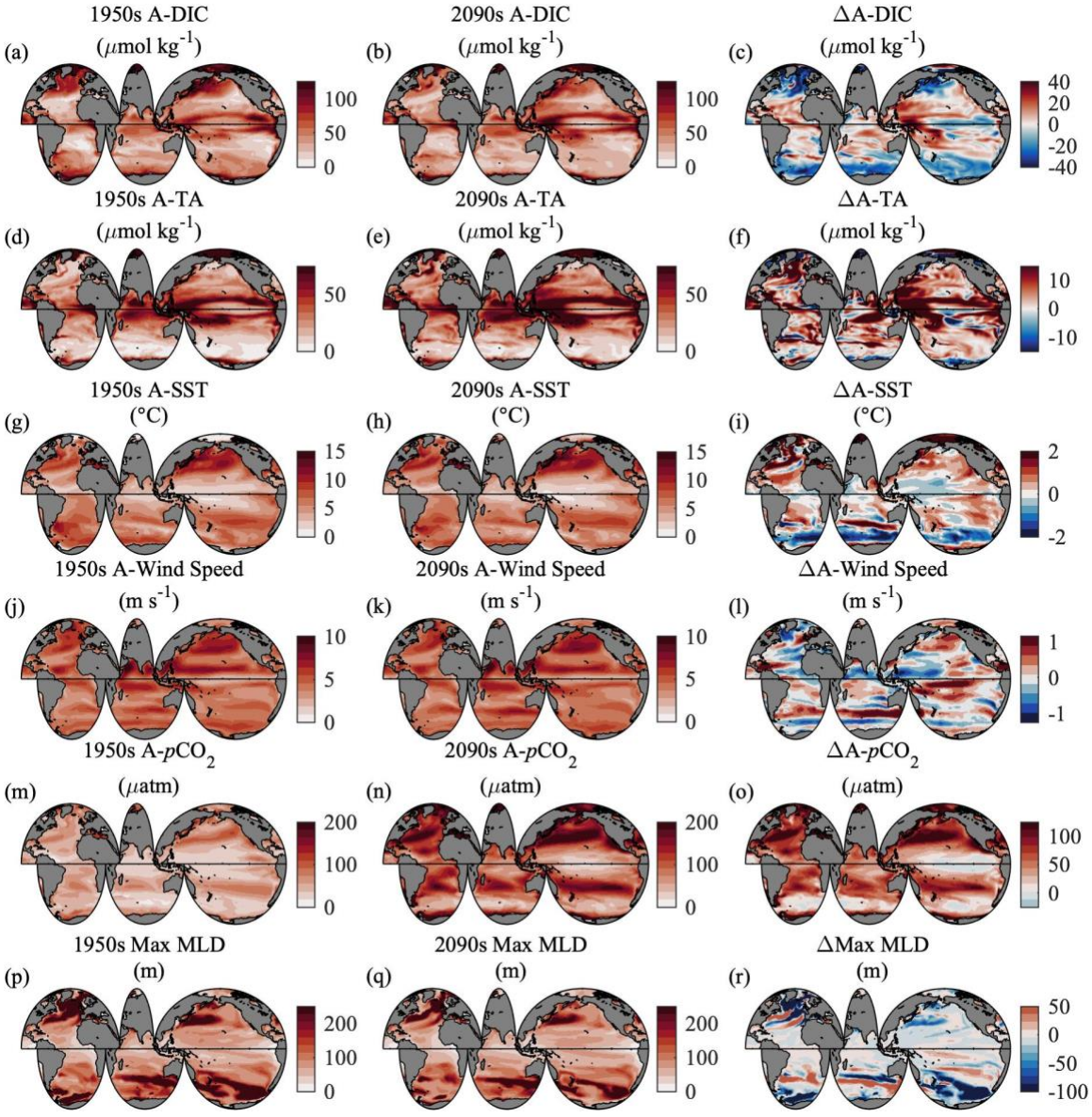

Figure S8. Average 1950s and 2090s seasonal cycle amplitudes (A) and the 1950s to 2090s change (Δ) in seasonal cycle amplitude for (**a-c**) dissolved inorganic carbon (DIC), (**d-f**) total alkalinity (TA), (**g-i**) sea surface temperature (SST), (**j-l**) wind speed, and (**m-o**) pCO_2. (**p-q**) Average 1950s and 2090s maximum mixed layer depth (MLD) and (**r**) the 1950s to 2090s change in maximum MLD. Ensemble mean result shown.

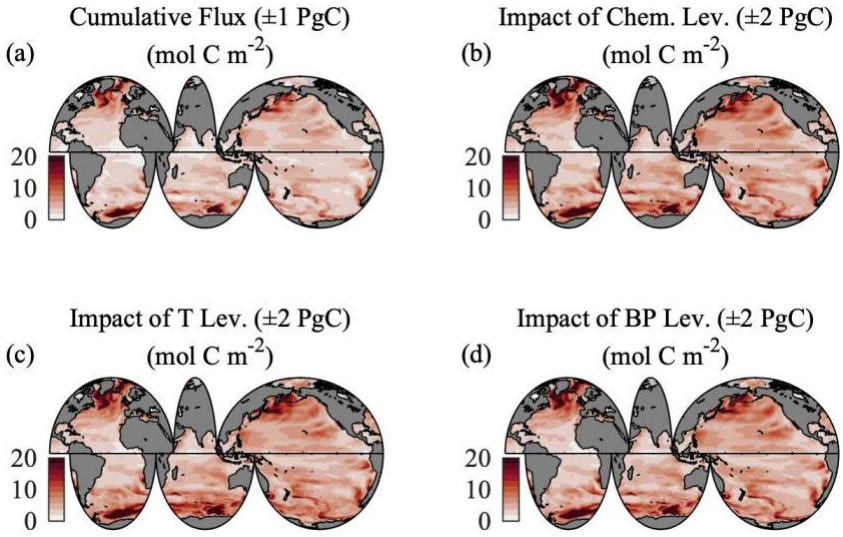

Figure S9. Standard deviation across ensemble members for (**a**) the transient cumulative flux and (**b**) the difference between the transient cumulative flux and the cumulative flux with no anthropogenic chemical leverage (Ø). Standard deviation across ensemble members for the configurations in which the impact of (**c**) thermal component chemical leverage and (**d**) biophysical component chemical leverage was added to the no leverage configuration. Values in the subplot tiles give the standard deviation across ensemble members for cumulative, globally integrated carbon uptake in units of PgC.

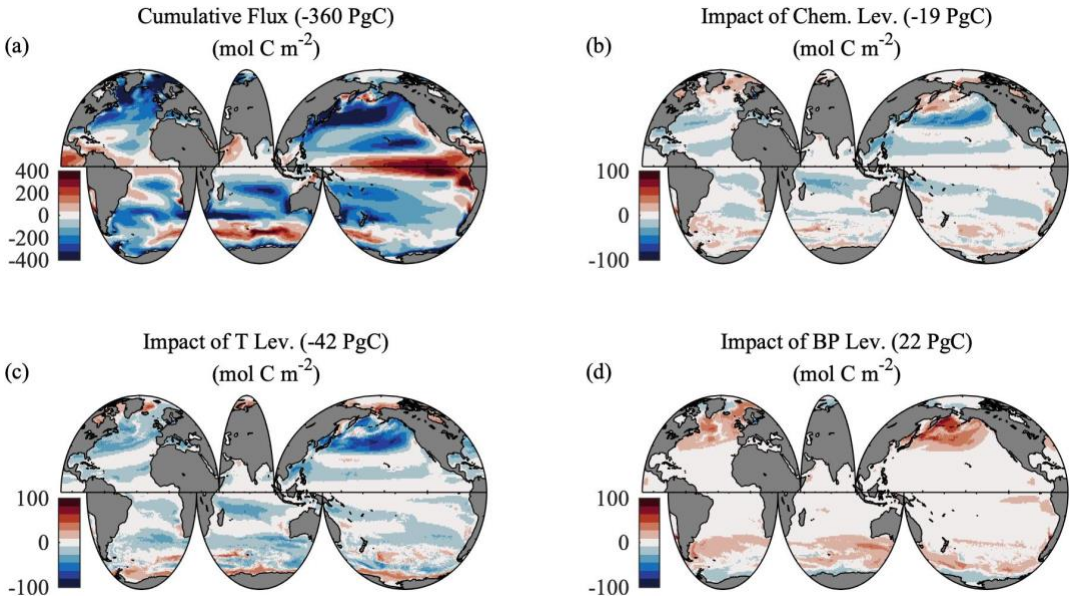

Figure S10. Results from ESM2M RCP4.5 scenario analysis. (**a**) Transient cumulative (1950 to 2100) flux and the (**b**) difference between the transient cumulative flux and the cumulative flux with no anthropogenic chemical leverage. Impact of adding (**c**) thermal component and (**d**) biophysical component chemical leverage to the no leverage configuration. For **b** through **d**, red colors indicate a weaker sink (or stronger source) and blue colors indicate a stronger sink (or weaker source) relative to the no-leverage configuration. Globally integrated values given in PgC.

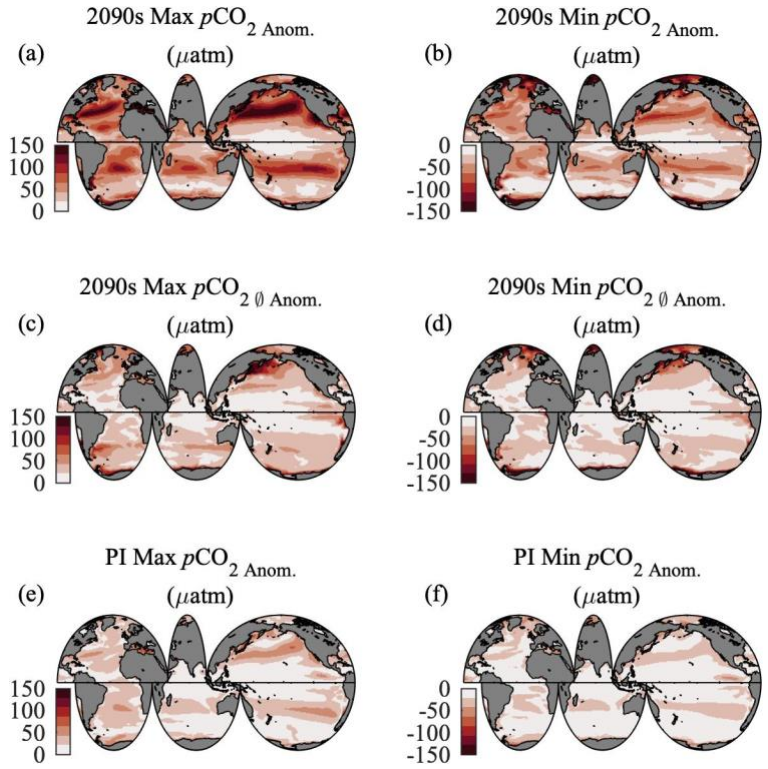

Figure S11. Maximum and minimum pCO_{2} anomalies (Anom.) relative to $pCO_{2\ AM}$ (µatm) for the 2090s (**a, b**) transient and (**c, d**) no chemical leverage (Ø) configurations as well as the (**e, f**) PI period. Ensemble mean result shown.

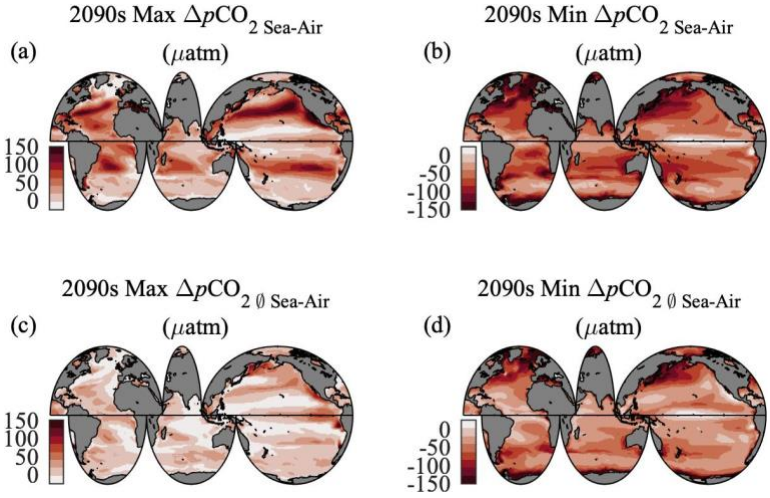

Figure S12. 2090s maximum and minimum $\Delta pCO_{2\ Sea-Air}$ values (µatm) for the (**a, b**) transient and (**c, d**) no chemical leverage (Ø) configurations. **Figure 6a-b** in the manuscript shows the difference between the left and right subplots. Ensemble mean result shown.

References Cited

van Heuven, S. M. A. C., Pierrot, D., Rae, J. W. B., Lewis, E., & Wallace, D. W. R. (2011). MATLAB program developed for CO_2 system calculations. *ORNL/CDIAC-105b. Carbon Dioxide Information Analysis Center, Oak Ridge National Laboratory, U.S. Department of Energy, Oak Ridge, Tennessee*. https://doi.org/10.3334/CDIAC/otg.CO2SYS_MATLAB_v1.1

Lewis, E., & Wallace, D. W. R. (1998). Program developed for CO_2 system calculations. *Carbon Dioxide Information Analysis Center, Oak Ridge National Laboratory, U.S. Department of Energy, Oak Ridge, Tennessee. Environmental Sciences Division. Publication No. 4735*. ORNL/CDIAC-105. https://doi.org/4735

Monteiro, P. M. S., Gregor, L., Lévy, M., Maenner, S., Sabine, C. L., & Swart, S. (2015). Intraseasonal variability linked to sampling alias in air-sea CO_2 fluxes in the Southern Ocean. *Geophysical Research Letters*, *42*(20), 8507–8514. https://doi.org/10.1002/2015GL066009

Wanninkhof, R. (2014). Relationship between wind speed and gas exchange over the ocean revisited. *Limnology and Oceanography: Methods*, *12*(JUN), 351–362. https://doi.org/10.4319/lom.2014.12.351

Weiss, R. (1974). Carbon dioxide in water and seawater: the solubility of a non-ideal gas. *Marine Chemistry*, *2*(3), 203–215. https://doi.org/10.1016/0304-4203(74)90015-2

Weiss, R. F., & Price, B. A. (1980). Nitrous oxide solubility in water and seawater. *Marine Chemistry*, *8*, 347–359.